Chinese Journal of
POLYMER SCIENCE

RESEARCH ARTICLE

https://doi.org/10.1007/s10118-026-3673-y
Chinese J. Polym. Sci.

Tuning the Structure and Properties of Poly(ethylene terephthalate)/Poly(butylene terephthalate) Blend Monofilaments: Mechanism of Transesterification and Gradient Structure Development

Zhong-Li Zhang[a,b], Bo-Hao Li[a,b], Jia-Ke Fan[a,b], Kang Chen[a,b*], Yi-Ning Hao[a,b], Xin-Yu Liu[a,b], and Xian-Ming Zhang[a,b]

[a] *School of Materials Science and Engineering, Zhejiang Sci-Tech University, Hangzhou 310018, China*
[b] *Zhejiang Provincial Innovation Center of Advanced Textile Technology, Shaoxing 312030, China*

Electronic Supplementary Information

Abstract To address the limited toughness of poly(ethylene terephthalate) (PET) monofilaments arising from the inherent molecular chain rigidity, this study prepared PET/poly(butylene terephthalate) (PBT) blend monofilaments *via* the melt-blend spinning method to enhance their toughness. The influence of PBT content on the structural evolution and properties of the blend system was systematically investigated. These results indicate that the PBT content significantly influences the extent of transesterification and compatibility, thereby dictating the mechanical behavior of the monofilaments. At a low PBT content of 2 wt%, transesterification was negligible. The monofilaments exhibited a uniform radial gradient orientation without a distinct skin-core structure, demonstrating optimal overall mechanical performance with markedly improved strength. Specifically, the tensile, loop, and knot strengths were 611, 421, and 443 MPa, respectively. When the PBT content exceeded 5 wt%, the flexible chain segments of PBT enhanced the molecular chain mobility in the blend chips, leading to an increase in crystallite size. However, intensified transesterification concurrently reduces the crystallizability and degrades the mechanical properties. At PBT contents above 15 wt%, SEM analysis revealed phase separation and pronounced heterogeneity in the radial gradient structure of the blend monofilaments, resulting in a significant deterioration of the mechanical properties. This study elucidates the pivotal role of blending ratio in governing the "composition-structure-property" relationship of PET/PBT-blended monofilaments, revealing the underlying mechanism of transesterification and gradient structure development. These findings provide a theoretical foundation for the design of high-performance PET monofilaments.

Keywords Poly(ethylene terephthalate) monofilament; Gradient structure; Melt-blend spinning

Citation: Zhang, Z. L.; Li, B. H.; Fan, J. K.; Chen, K.; Hao, Y. N.; Liu, X. Y.; Zhang, X. M. Tuning the structure and properties of poly(ethylene terephthalate)/poly(butylene terephthalate) blend monofilaments: mechanism of transesterification and gradient structure development. *Chinese J. Polym. Sci*. https://doi.org/10.1007/s10118-026-3673-y

INTRODUCTION

Polyester monofilaments particularly those made from poly(ethylene terephthalate) (PET) are widely used in knitted spacer fabrics, woven belts, filtration, and printing screens because of their excellent mechanical properties, dimensional stability, and cost-effectiveness processability.[1–3] With the expanding application of PET monofilaments in advanced fields, such as flexible electronics and wearable devices, there is a growing demand for improved toughness and bending endurance. However, the inherent rigidity and low toughness of PET molecular chains limit their further applications.[4] Therefore, enhancing the toughness of monofilaments is an urgent issue that needs to be addressed.

Various modification methods have been developed to enhance the toughness of PET. Blending technology has drawn considerable attention owing to its efficiency, cost-effectiveness, and simple processing, which allows for effective regulation of comprehensive properties while largely preserving the fundamental performance of PET.[5–8] In the early stage, the incorporation of elastomers as a dispersed phase was one of the primary approaches to toughening. For example, Tan *et al*.[9] employed glycidyl methacrylate (GMA)-functionalized ethylene-propylene-diene monomer rubber (EPDM-*g*-GMA), achieving a brittle-ductile transition in the blend system at a rubber proportion of 20 wt%. The impact strength increased significantly from 17 J/m for neat PET to 840 J/m, representing an enhancement of over 4900%. However, the generally poor compatibility between elastomers and the PET matrix often results in weak interfacial adhesion, leading to reduced monofilament strength and fibrillation.

* Corresponding author, E-mail: chenkang@zstu.edu.cn
Received February 8, 2026; Accepted March 30, 2026; Published online July 15, 2026

Blending and spinning with the same type of raw materials offers a feasible alternative to address compatibility issues. For instance, Mazraeh-Shahi *et al.*[10] used two polypropylene materials with different molecular weight distributions for spinning and achieved improved toughness in polypropylene fibers through gradient structural control. Nevertheless, this method is limited to adjusting the compatibility *via* molecular weight and its distribution, which inherently limits the scope of tunability. Therefore, the selection of polymers with chemical structures similar to PET, such as poly(trimethylene terephthalate) (PTT), thermoplastic polyester elastomer (TPEE), and poly(butylene terephthalate) (PBT), represents a more promising strategy for toughening while ensuring spinnability and compatibility. Among these, PBT is considered an ideal candidate for toughening PET because of its similar chemical structure, which promotes compatibility, as well as its lower glass transition temperature, excellent inherent toughness, and favorable processability.[11–13] Extensive research has been conducted on PET/PBT blended systems. For example, Avramov *et al.*[14] reported a single glass transition temperature in PET/PBT blends, indicating good compatibility between PET and PBT segments in the amorphous phase. Subsequently, Aravinthan *et al.*[15] investigated the effect of blending ratio on impact performance and found that PET/PBT blends with different ratios exhibited superior impact resistance and toughness compared to either neat component. Although previous studies have extensively examined PET/PBT blends, including the transesterification reaction that occurs during blending,[16] the preparation of PET/PBT blend monofilaments and the systematic regulation of their structures and properties have not been sufficiently explored.

During the preparation of blend monofilaments, factors such as non-uniform distributions of the temperature field, stress field, and strain lead to significant structural differences along the radial direction of the monofilaments.[17] The precise characterization of the radial gradient structure remains a considerable technical challenge owing to the small diameter of the monofilaments. In recent years, advances in advanced characterization techniques, particularly synchrotron radiation, have provided strong support. Pan *et al.*[18] applied synchrotron radiation micro-beam X-ray diffraction to study the radial crystallization differences in polypropylene (PP) fibers. The results indicated that the non-uniform radial temperature distribution during melt-spinning led to higher crystallinity in the central region compared with the surface. Subsequently, Davies *et al.*[19] utilized synchrotron-based microfocus X-ray diffraction to quantitatively analyze changes in the crystalline orientation between the skin and core layers of poly(*p*-phenylene benzobisoxazole) (PBO) fibers. Furthermore, Perret *et al.*[20] successfully resolved the radial crystallinity gradient in PET monofilaments by combining high-resolution Raman imaging with micro-beam small-angle X-ray scattering tomography.

Although several studies have investigated the toughening modification of PET, most have focused on bulk materials prepared by compression or injection molding, with limited attention paid to improving the toughness of monofilaments. Therefore, this study modifies PET monofilaments by introducing toughness PBT, with a focus on its effect on toughness. PET/PBT composite monofilaments were prepared by melt-blending extrusion. The influence of PBT content on the thermal stability, mechanical properties, and toughness was systematically investigated. Furthermore, the radial structural heterogeneity of the monofilaments was examined to elucidate the underlying performance mechanisms, thereby providing crucial scientific insights for process optimization. This research not only broadens the application scope of PET monofilaments but also offers theoretical and experimental foundations for the design and preparation of high-performance fibers.

EXPERIMENTAL

Materials

The high-viscosity PET chips used in the experiment were purchased from Zhejiang Unifull Industrial Fiber Co., Ltd., with a melting temperature (T_m) of 249 °C, glass transition temperature (T_g) of 64 °C, and intrinsic viscosity of 1.1 dL/g (in phenol/1,1,2,2-tetrachloroethane mixed solvent (1/1, *W*/*W*) at 25 °C). PBT chips were purchased from Suzhou Poly Plastic Masterbatch Co., Ltd., China, with a T_m of 227 °C, a T_g of 47 °C, and an intrinsic viscosity of 1.0 dL/g (in phenol/1,1,2,2-tetrachloroethane mixed solvent (1/1, *W*/*W*) at 25 °C).

Preparation of PET/PBT Blended Chips

To enhance the blending homogeneity and prevent hydrolysis during processing, the drying procedure consisted of a combined atmospheric and vacuum drying step at 110 °C for a total duration of 12 h to ensure sufficient moisture removal. The mass ratios of PET/PBT investigated in this study were 100/0, 98/2, 95/5, 90/10, 85/15, 75/25, 65/35, 50/50, and 0/100. The corresponding samples were designated PET, PET/PBT-2%, PET/PBT-5%, PET/PBT-10%, PET/PBT-15%, PET/PBT-25%, PET/PBT-35%, PET/PBT-50%, and PBT, respectively.

Melt blending of the dried samples was performed using a laboratory-scale twin-screw extruder (SJZS-10B, Wuhan Ruiming Experimental Instrument Manufacturing Co., Ltd., China). A schematic illustrating the preparation of the PET/PBT-blended chips is shown in Fig. 1. For neat PET and PET/PBT, the temperature profiles of the three heating zones were set as 255, 260, and 265 °C, respectively. For neat PBT, the temperatures were set to 225, 230, and 235 °C.

Preparation of PET/PBT Monofilaments

The blended chips obtained were transferred to a bench-scale vertical extruder (WJSLX-10, Shanghai Xinshuo Precision Machinery Co., Ltd., China). The specific process parameters were as follows: spinning temperature of 270 °C and extrusion rate of 5–6 mm/min. The as-spun monofilaments were prepared at a drawing speed of 54.7 m/min.

The as-spun f monofilaments were drawn according to the parameters listed in Table 1, and a schematic diagram of the spinning and drawing processes is shown in Fig. 2.

Characterizations

Differential scanning calorimetry (DSC)

The thermal properties of the PET/PBT-blended chips were characterized using DSC (DSC3, Mettler-Toledo, Switzerland). Samples weighing approximately 5–10 mg were sealed in aluminum crucibles and tested under nitrogen atmosphere at a

https://doi.org/10.1007/s10118-026-3673-y

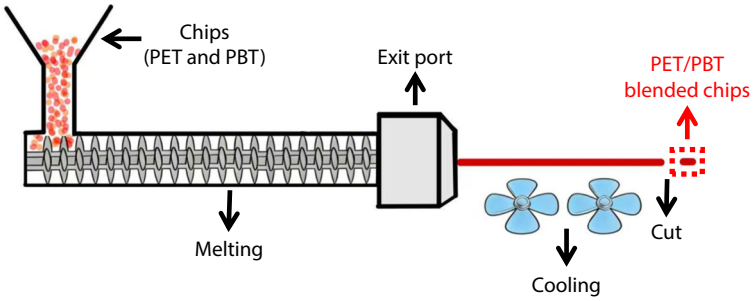

Fig. 1 Schematic diagram of the preparation of PET/PBT blended chips.

Table 1 Parameters for the drawing process of PET/PBT monofilaments.

Drawing	Temperature (℃)	Godet 1 (m/min)	Take-up (m/min)	Draw ratio
First-stage	100	5.5	16.4	3
Second-stage	100	5.5	11.0	2

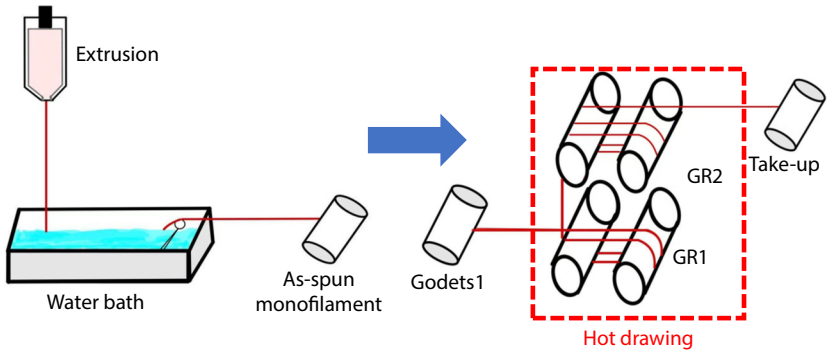

Fig. 2 Schematic diagram of the preparation of PET/PBT monofilaments.

flow rate of 50 mL/min. The temperature program consisted of heating from 30 ℃ to 280 ℃ at a rate of 10 ℃/min.

Carbon nuclear magnetic resonance spectroscopy (^{13}C-NMR)

The blended chips were analyzed using liquid-state nuclear magnetic resonance (400 MHz, Bruker, Germany). For the measurement, 40 mg of the sample was dissolved in deuterated trifluoroacetic acid (0.5 mL), with tetramethylsilane (TMS) as the internal standard.

Mechanical test

The mechanical properties of the monofilaments were evaluated using an electronic single-yarn tensile tester (YG020B, Changzhou Textile Instrument Co., Ltd., China). All tests were conducted under standard conditions (25 ℃, 65% RH) with a gauge length of 100 mm and tensile speed of 100 mm/min. Each test was repeated five times, and the average value was calculated.

Intrinsic viscosity test

A precisely weighed sample (0.125 g) was dissolved in 25 mL of phenol/1,1,2,2-tetrachloroethane mixed solvent (1/1, *W*/*W*). Intrinsic viscosity was determined using a Ubbelohde viscometer. The measurements were repeated thrice, and the average value was calculated. The intrinsic viscosity [η] of the samples was calculated using Eq. (1):

$$[\eta] = \frac{\sqrt{2\left(\eta_{sp} - \ln\eta_r\right)}}{C} \quad (1)$$

where $\eta_r = t/t_0$ is the relative viscosity, $\eta_{sp} = \eta_r - 1$ is the specific viscosity, t is the flow time of the solution, t_0 is the flow time of the solvent, and c is the concentration of the solution (g/dL).[21]

Dynamic mechanical analysis (DMA)

The loss tangent (tanδ) versus temperature curves of the monofilaments were obtained using DMA (DMA 1, Mettler-Toledo, Switzerland). The measurements were performed in the tensile mode under the following conditions: a frequency of 1 Hz, an amplitude of 10 μm, a temperature range from 30 ℃ to 220 ℃, and a heating rate of 3 ℃/min.

Scanning electron microscopy (SEM)

The surface and cross-sectional morphologies of the monofilaments were observed by SEM (SEM; Sigma 500, Zeiss, UK). Prior to observation, the samples were sputter-coated with gold using an ion-sputter coater. The experiments were performed at an accelerating voltage of 1.5 kV under a nitrogen atmosphere with magnifications of 500× and 8000×.

Wide-angle x-ray diffraction (WAXD)

WAXD experiments were performed at the BL14B1 beamline of the Shanghai Synchrotron Radiation Facility (SSRF). The incident X-ray wavelength was 0.0688 nm and the sample-to-detector distance was set at 493.18 mm. The obtained two-dimensional WAXD (2D WAXD) patterns were processed using X-polar software (Percision Works NY, Inc., USA) based on a two-phase structural model to extract parameters including the crystallite size and crystalline orientation factor.[22–24]

Small-angle X-ray scattering (SAXS)

SAXS experiments were performed at the BL16B1 beamline of the Shanghai Synchrotron Radiation Facility (SSRF). The X-ray wavelength was set to 0.124 nm with a sample-to-detector distance of 2070 mm. Two-dimensional SAXS (2D SAXS) patterns were collected using a PILATUS3 2M detector and subsequently processed with X-polar software (Percision Works NY, Inc., USA) to obtain structural parameters such as lamellar thickness and long period.[25–27]

Confocal Raman spectrometer testing (CRM)

The monofilaments were analyzed using CRM (inVia Qontor, Renishaw, UK). A 532 nm laser source was employed through a 50× objective lens. The measurements were performed with a laser power of 1 mW and accumulation time of 30.0 s.

RESULTS AND DISCUSSIONS

Effect of PBT Content on the Properties of the Blended Chips

The high chemical structural similarity between PET and PBT results in good compatibility. Their blends undergo transesterification when heated above the T_m.[28] To investigate the influence of the blending ratio on this reaction in PET/PBT blended chips and evaluate the compatibility between the components during blending, the chips were systematically characterized using NMR and DSC.

Transesterification produces copolymers characterized by non-uniform alkylene chain lengths, which alter the electron cloud density around the aromatic quaternary carbon atoms and ultimately give rise to new aromatic quaternary carbon peaks in the NMR spectrum at the characteristic chemical shift of approximately 133.7 ppm.[29,30] Therefore, the occurrence of transesterification during blending can be directly determined by detecting the presence of the aromatic quaternary carbon peak at 133.7 ppm in the blended chips. As shown in the ^{13}C-NMR spectra of PET/PBT blended chips (Fig. 3), corresponding to the aromatic quaternary carbon of the transesterification product, becomes evident when the PBT content exceeds 2 wt%, confirming the occurrence of transesterification. The intensity of this aromatic quaternary carbon resonance peak increased with increasing PBT content in the blend. However, when the PBT content was ≤2 wt%, this characteristic peak was not detected, suggesting that no significant transesterification occurred in the system.

To further elucidate the impact of the PBT content on the thermodynamic properties, DSC was employed to analyze the PET, PBT, and PET/PBT blended chips. The first-heating DSC curves and the corresponding thermodynamic parameters are presented in Fig. 4 and Table 2, respectively. A single T_g can be observed for all the blended samples, confirming the good compatibility between PET and PBT in the amorphous region. When the PBT content is ≤15 wt%, the blends exhibit only a single melting peak. As the PBT content increases, this peak gradually shifts towards lower temperatures and broadens Specifically, the T_m-II decreases from 257.3 °C for neat PET to 256.2 °C for the PET/PBT-15%. When the PBT content exceedes 15 wt%, two distinct melting peaks emerged, corresponding to PET- and PBT-rich crystalline domains, indicating deteriorated crystalline phase compatibility at higher PBT levels.[31,32] Concurrently, T_m-I of the PBT component further decreases from 221.83 °C to 220.67 °C as its content increases. The observed changes in the melting behavior can be attributed to transesterification during the blending of PET and PBT. The block copolymers generated by this reaction disrupt the regularity of the molecular chains and broaden the molecular weight distribution, ultimately reducing the crystallization ability of the blends.[33,34]

In summary, the NMR and DSC results collectively demonstrate that the PBT content directly governs the extent of transesterification, which, in turn, governs the final material properties. At low PBT contents (≤2 wt%), transesterification was negligible, and the blends maintained a good amorphous phase compatibility. As PBT increased (≤15 wt%), transesterification intensified, and the generated copolymers disrupted chain regularity, macroscopically lowering both the perfection and capacity of crystallization. At higher PBT levels

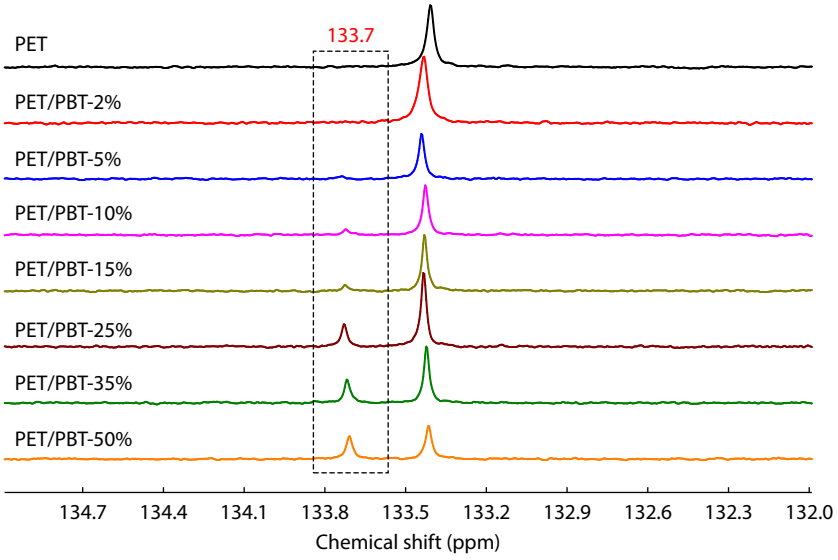

Fig. 3 ^{13}C-NMR spectra of PET/PBT blended chips.

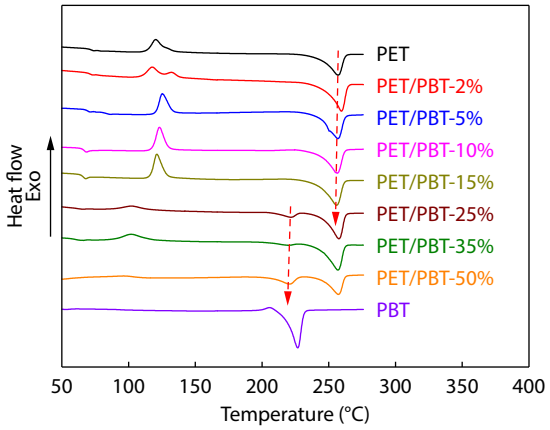

Fig. 4 DSC heating curves of PET/PBT blended chips.

(>15 wt%), in addition to pronounced transesterification, kinetic competition during crystallization leads to separate nucleation, forming incompatible crystalline regions.

Properties and Structures of PET/PBT Monofilaments

The aforementioned study on PET/PBT blended chips confirmed their good compatibility at low PBT contents, laying a solid theoretical basis for subsequent work. PET/PBT monofilaments were further prepared *via* a melt spinning process to systematically investigate the influence of PBT content on the structure and properties of the monofilaments.

Table 2 Thermal parameters of PET/PBT blended chips.

Sample	T_g (°C)	T_m-I (°C)	T_m-II (°C)
PET	71.6	–	257.3
PET/PBT-2%	71.0	–	259.5
PET/PBT-5%	68.5	–	257.3
PET/PBT-10%	65.8	–	256.7
PET/PBT-15%	64.7	–	256.2
PET/PBT-25%	63.6	221.8	257.8
PET/PBT-35%	61.3	219.8	257.2
PET/PBT-50%	54.5	220.7	257.3
PBT	53.1	–	227.0

Mechanical properties

The mechanical properties of the monofilaments were tested at room temperature, and shown in Fig. 5(a). The results show that as the PBT proportion increases, the tensile strength of the monofilaments exhibits a trend of initially increasing slightly and then gradually decreasing. When the PBT proportion is 2 wt%, the PET/PBT monofilaments achieve the highest tensile strength, indicating that the incorporation of a small amount of PBT has a positive effect on the tensile strength. However, as the

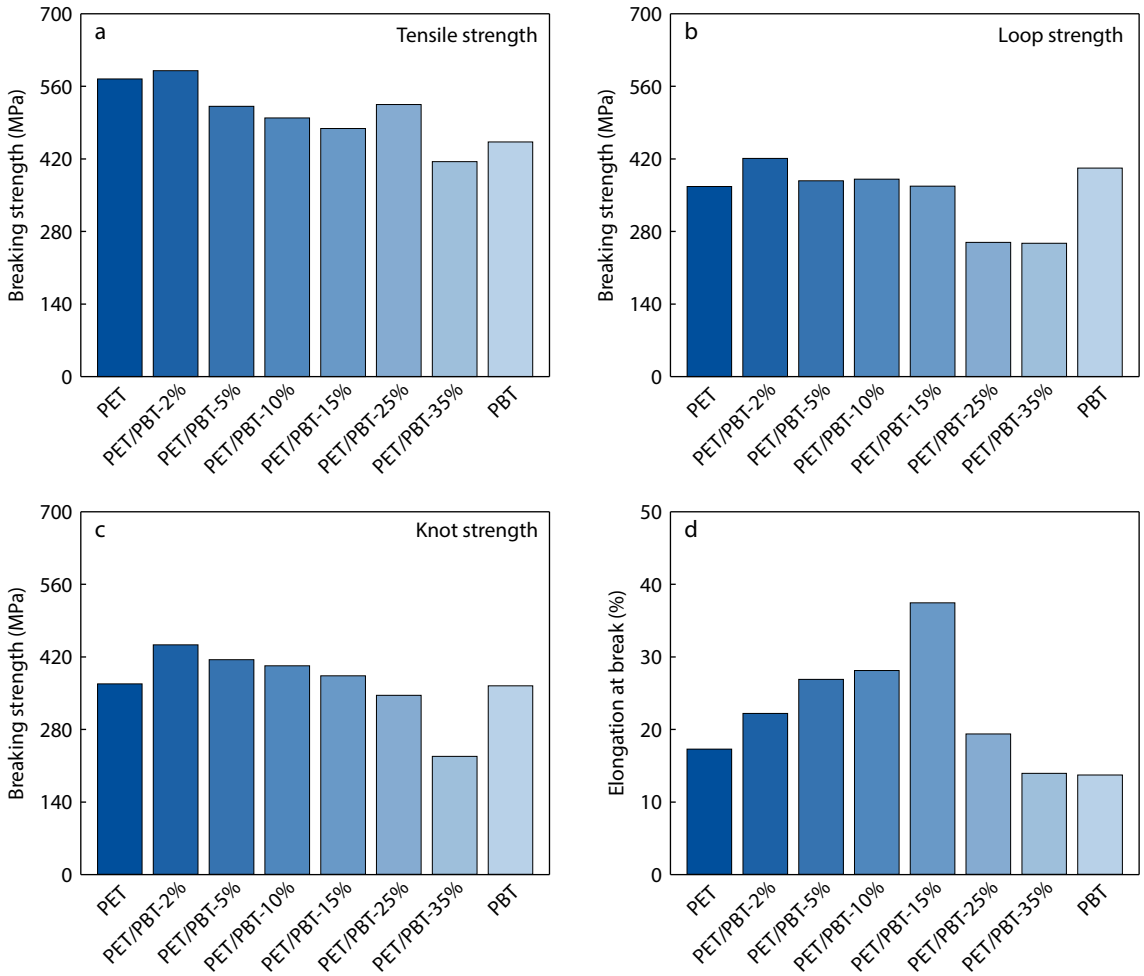

Fig. 5 (a) Tensile strength, (b) loop strength, (c) knot strength, and (d) elongation at break values of PET/PBT monofilaments.

https://doi.org/10.1007/s10118-026-3673-y

PBT proportion further increases, especially when it exceeds 15 wt%, the tensile strength decreases significantly. This decline may be attributed to phase separation induced by excessive PBT or impaired crystalline integrity resulting from ester exchange reactions.

The loop strength (Fig. 5b) and knot strength (Fig. 5c), which are important parameters for characterizing the toughness of monofilaments, exhibited similar trends. Overall, it shows a slight increase followed by a gradual decline. As the PBT content continued to increase, the strength progressively declined. This indicates that an appropriate amount of PBT helps maintain the local stress transfer capability of the monofilament, while an excessively high ratio (>15 wt%) may lead to easier failure at loops or knots owing to phase separation or deteriorated structural uniformity.

The elongation at break (Fig. 5d) reflects the deformability of the blended monofilaments. When the PBT content was ≤ 15 wt%, the elongation at break generally exhibited an increasing trend. This result indicates that the incorporation of PBT improved the toughness of the material to a certain extent, enabling it to withstand greater plastic deformation during tensile loading. However, when the PBT content exceeded 15 wt%, the elongation at break decreased markedly, which is attributed to the increased transesterification and phase separation at higher PBT loadings.

In summary, the incorporation of PBT exerted a significant tuning effect on the mechanical properties of PET monofilaments. At low addition levels (≤2 wt%), the overall performance of the monofilaments was enhanced to a certain extent. However, as the PBT content increased further, although the elongation at break improved, the various strength indicators declined. This reflects the transition of the material from a "rigidity-dominant" to a "toughness-oriented" characteristic. This transition is closely related to the compatibility level between PET and PBT, the extent of transesterification, and the consequent changes in the crystalline structure and interfacial bonding state, which are investigated in detail in the following sections. Notably, the PET/PBT-2% monofilament achieved an optimal balance between high strength and good toughness. In weaving applications, it effectively resists repeated bending and friction in high-speed looms, reducing breakage rates and improving the weaving efficiency.[35] The excellent knot strength of fishing nets enables plastic deformation in the knot area to dissipate stress, thereby delaying fracture and extending service life in marine environments.[36]

Chemical structure

The intrinsic viscosity of the PET/PBT monofilaments, which correlates with the average molecular weight, remained largely unchanged with increasing PBT content (Table 3). This indicates that the molecular weight of the blends was not compromised, and thus the variations in mechanical properties were attributable to structural and morphological changes rather than molecular weight reduction.

Supramolecular structure

The molecular chain mobility within the amorphous regions of the monofilaments was evaluated by DMA. The DMA curves are shown in Fig. 6.

All monofilaments exhibited a single T_g, confirming the good compatibility between PET and PBT in the amorphous phase. The T_g significantly decreased with increasing PBT content. Specifically, it dropped from 130.1 °C for neat PET monofilaments to 108.3 °C for the PET/PBT-35% blend. This reduction indicates a lower energy barrier for segmental motion and enhanced chain mobility in amorphous regions. The observed decrease in T_g was attributed to two main factors. First, the α segments in the PBT chains have an inherently lower rotational energy barrier than those in PET, which fundamentally enhances the segmental mobility of the blend. Second, transesterification between PET and PBT generates block copolymers that further promote chain mobility.[31,37]

Table 3 Intrinsic viscosities of PET/PBT monofilaments.

Sample	Intrinsic viscosity (dL/g)
PET	0.63
PET/PBT-2%	0.65
PET/PBT-5%	0.68
PET/PBT-10%	0.69
PET/PBT-15%	0.71
PET/PBT-25%	0.76
PET/PBT-35%	0.79
PBT	0.79

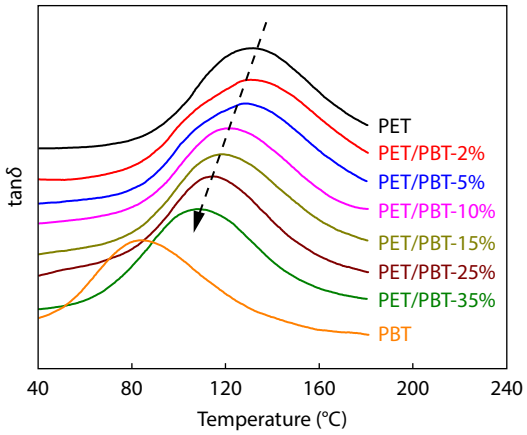

Fig. 6 DMA curves of PET/PBT monofilaments.

To further investigate the evolution of the crystal structure in the PET/PBT monofilaments, 2D WAXD tests were performed, and the results are shown in Fig. 7(a). Because of the similar crystal structures of PET and PBT, some of their characteristic diffraction peaks are located close to each other, making it difficult to distinguish clearly in the 2D WAXD patterns.[38] For all PET/PBT monofilaments, the positions of the characteristic diffraction peaks in the 2D WAXD patterns remained essentially consistent with those of the PET monofilaments, and no independent diffraction signals corresponding to new crystalline phases were detected.[39] 1D integral patterns along the equatorial direction are shown in Fig. 7(b). The positions of the characteristic diffraction peaks of all the blended monofilaments showed no significant shift compared with those of neat PET.

Further quantitative analysis of the WAXD patterns was conducted to determine the crystallite size and crystalline orientation degree (f_c), and the results are shown in Fig. 7(c). When the PBT content was ≤5 wt%, the crystallite size of the PET/PBT monofilaments remained essentially unchanged compared to that of the PET monofilament. However, as the

https://doi.org/10.1007/s10118-026-3673-y

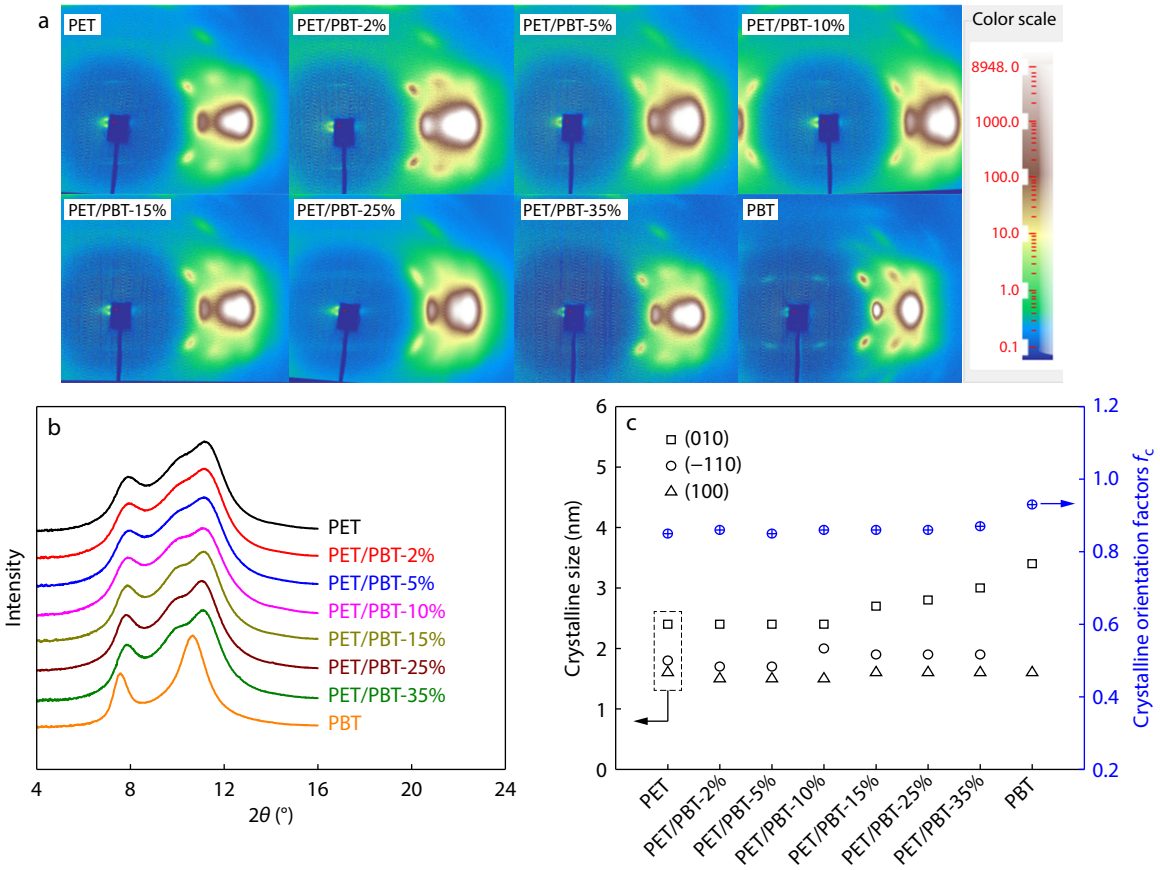

Fig. 7 (a) 2D WAXD patterns, (b) 1D integral patterns along the equatorial direction, (c) crystalline sizes and crystalline orientation factors of PET/PBT monofilaments.

PBT content increased to 35 wt%, the crystallite sizes of the (010), (−110), and (100) planes increased from 2.4 nm, 1.7 nm, and 1.5 nm to 3.0 nm, 1.9 nm, and 1.6 nm, respectively. This change is primarily attributed to the longer aliphatic methylene segments in the PBT chains, which impart a higher segmental mobility.[40] As the PBT content increases, the fraction of highly mobile segments increases, enhancing the overall segmental mobility and providing more favorable kinetic conditions for crystallite growth during spinning and drawing, thereby leading to enlarged crystallite sizes at higher PBT contents (>5 wt%). The PBT monofilament exhibits crystallite sizes of 3.4 nm for the (010) plane and 1.6 nm for the (100) plane, which are significantly larger than those of PET monofilament, directly reflecting its intrinsically higher segmental mobility.[41] In addition, the introduction of PBT had little influence on f_c of the blended monofilaments, which remained largely stable across all blend contents.

Lamellar structure

SAXS was employed to further investigate the influence of PBT content on the lamellar structure of PET/PBT monofilaments. The 2D SAXS patterns are shown in Fig. S1 (in the electronic supplementary information, ESI). Although both PET and PBT are semicrystalline polymers, their 2D SAXS profiles display distinct scattering characteristics. Pure PET monofilaments typically exhibit a "four-point" pattern along the meridional direction, whereas neat PBT shows a "two-point" scattering geometry.[41,42] As observed in Fig. S1 (in ESI), the PET/PBT monofilaments largely retain the "four-point" scattering signature. The integration of the lamellar scattering signals along the meridional direction yielded the corresponding 1D scattering intensity profiles and correlation functions, as shown in Fig. 8(a) and Fig. 8(b), respectively.

To further analyze the evolution of the lamellar structure, key parameters including the long period (L_M), lamellar thickness (L_A), amorphous thickness (L_N), lamellar diameter (L_E), and tilting angle (φ) were quantitatively derived from the SAXS data, as summarized in Fig. 8. In the PET/PBT monofilaments, the addition of PBT did not systematically alter these structural parameters. With increasing PBT content, L_A, L_N, L_M, and φ remained constant. This suggests that the core lamellar characteristics are dominated by the strong drawing conditions during spinning rather than by the PBT content. However, when the PBT content reached or exceeded 5 wt%, a modest increase in L_E can be observed. This can be attributed to changes in the melt rheology induced by PBT addition, which indirectly modified the spinning conditions and provided limited additional space for lateral lamellar growth.

Morphological changes

To examine the influence of the PBT content on the monofilament morphology, the surfaces of the samples can be observed using SEM at 500× magnification (Fig. 9a). The surface of the PET monofilaments appeared smooth and flat with no obvious defects or particulate matter. At low PBT contents (<15 wt%), the monofilament surface remained relatively smooth, indicating

https://doi.org/10.1007/s10118-026-3673-y

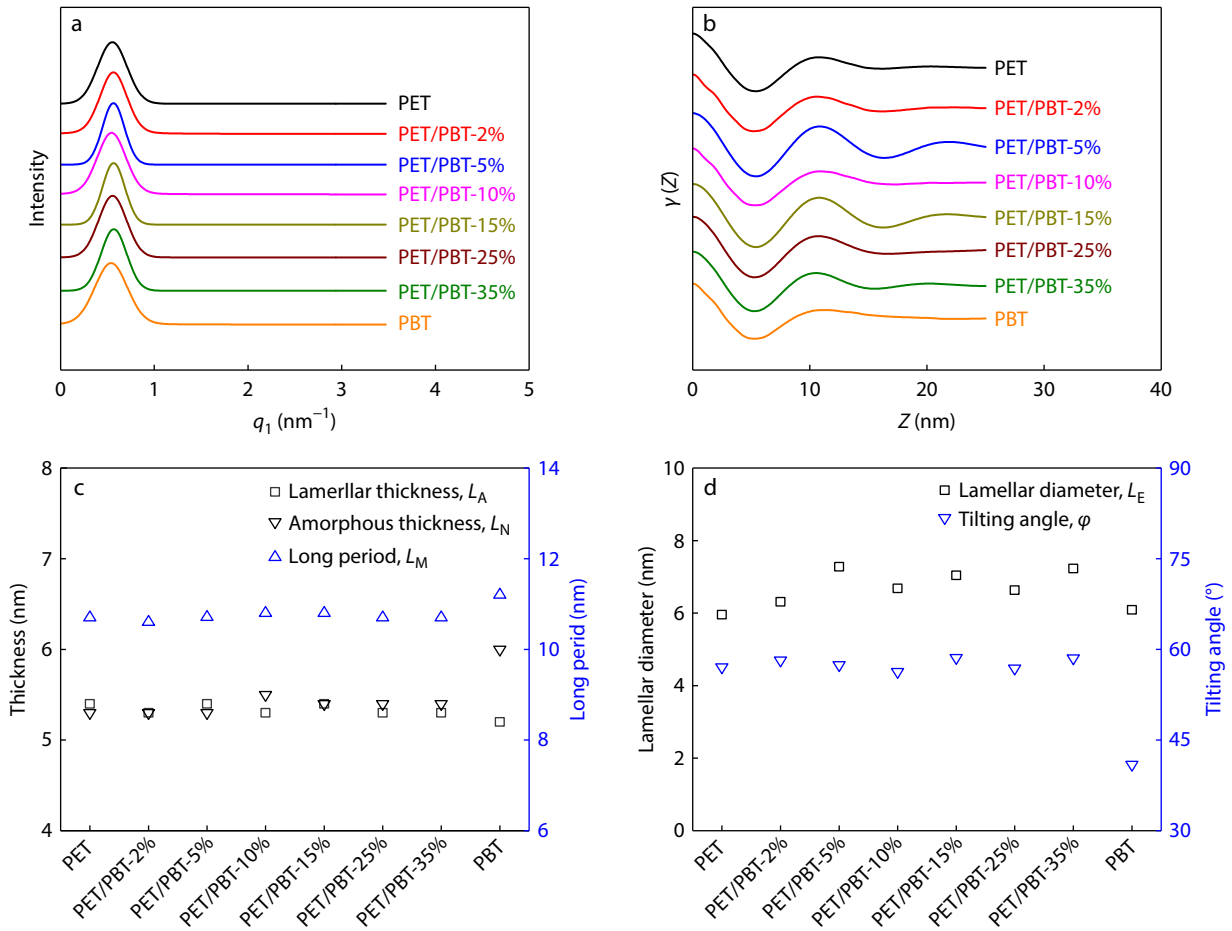

Fig. 8 (a) 1D scattering intensity distributions and (b) correlation function, (c, d) lamellar structural parameters of PET/PBT monofilaments.

that the phase separation was weak and that the changes in monofilament properties were predominantly dominated by transesterification. When the PBT content reached or exceeded 15 wt%, distinct plate-like surface defects became apparent, and the degree of phase separation between PET and PBT increased significantly, leading to considerable expansion of the defective surface area. Although transesterification continued, its destructive effect on the crystalline region was no longer the sole factor responsible for property degradation. Instead, the interfacial defects and stress concentration induced by phase separation became the dominant factors driving the further deterioration of the properties. SEM observations of the cross-sections (Fig. 9b) revealed a similar trend. When the PBT content exceeded 2 wt%, increased transesterification and intensified phase separation led to a significant increase in the defect density within the cross-sectional area. Taken together, these phenomena indicate that for PET/PBT monofilaments, transesterification and phase separation are coexisting and competing processes that collectively determine the final morphology and properties of the blend.

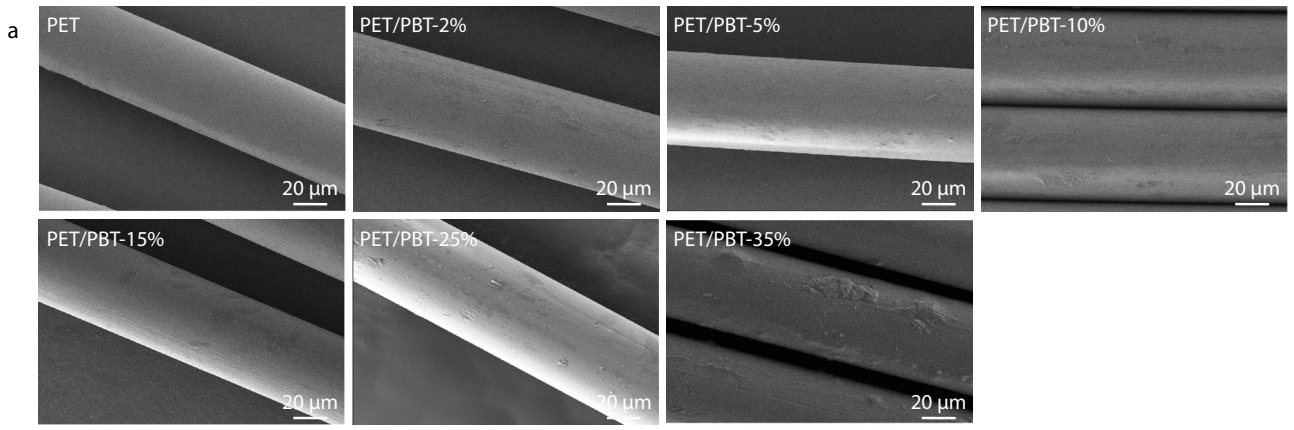

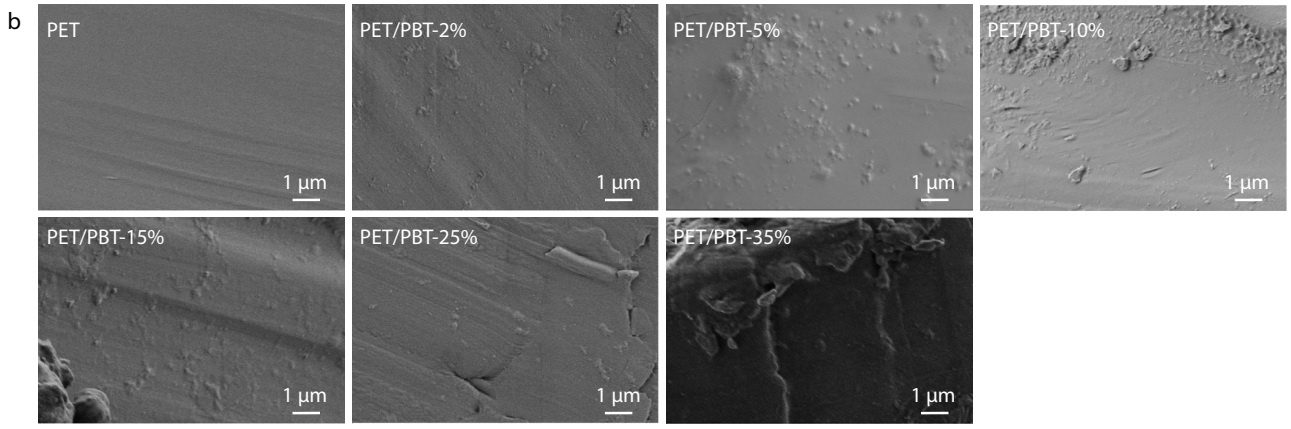

Fig. 9 (a) Surface morphologies and (b) cross-sectional morphologies of PET/PBT monofilaments.

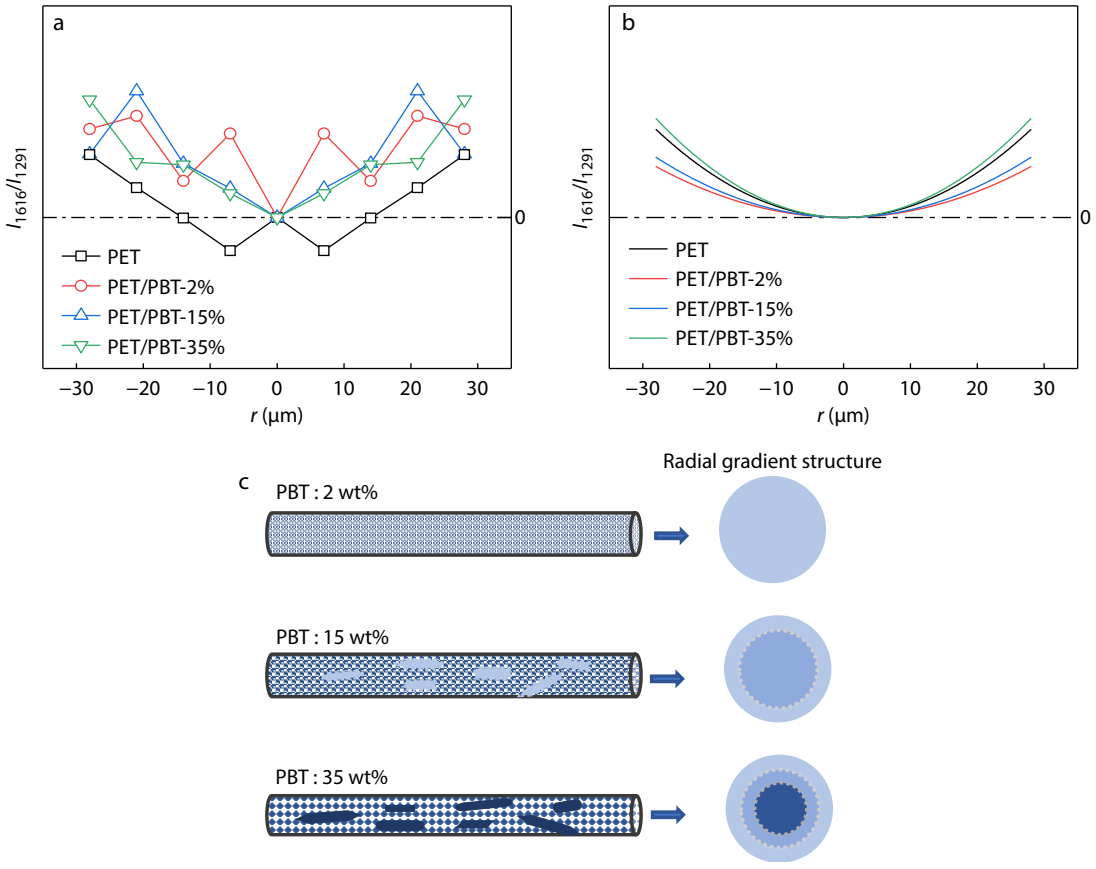

Fig. 10 Radial Raman analysis of PET/PBT monofilaments. (a) Distribution of intensity ratio differences of I_{1616}/I_{1291}; (b) Distribution of intensity ratio differences of I_{1616}/I_{1291} after smoothing; (c) Schematic diagram of radial structure gradient distribution.

Radial structure gradient distribution

To investigate the radial distribution of the molecular chain orientation in PET/PBT monofilaments, cross-sectional Raman spectroscopy was performed on four types of monofilaments: PET, PET/PBT-2%, PET/PBT-15%, and PET/PBT-35%. The raw Raman data are shown in Fig. S2 (in ESI). All Raman spectra were normalized using the stable methylene deformation vibration band at 1291 cm^{-1} as an internal reference.[43]

In Fig. 10, the intensity ratio at the core is defined as zero. The Raman band at 1616 cm^{-1} corresponds to the in-plane vibration mode of the benzene ring, whose intensity reflects the molecular chain orientation. The signal was strongest when the benzene ring plane was parallel to the laser polarization direction. If the molecular chains are highly oriented along the fiber axis, the benzene ring planes tend to align perpendicularly to the polarization direction, leading to a weaker signal. Thus, the intensity of this peak is negatively correlated with the degree of orientation. After baseline correction with reference to the core intensity, the radial gradient of the intensity difference was obtained (Fig. 10a). The re-

sults show that for all monofilaments, the peak intensity at 1616 cm^{-1} gradually increased from the core to the skin layer, indicating that the molecular chain orientation in the core region was significantly higher than that in the skin layer.

The smoothed distribution curves of the I_{1616}/I_{1291} intensity difference along the radial direction for PET/PBT monofilaments are shown in Fig. 10(b) and the schematic diagram of radial structural changes is shown in Fig. 10(c). The analysis revealed that the radial molecular chain orientation distribution was the most uniform when the PBT content was 2 wt%. However, once the PBT content exceeded this threshold (≥2 wt%), the non-uniformity of the radial orientation distribution increased significantly with higher PBT loading. This was attributed to the enhanced transesterification and more pronounced phase separation induced by excessive PBT, which led to greater fluctuations in the transmission of stress and temperature fields along the radial direction during drawing and cooling. A uniform radial orientation distribution corresponds to a continuous and gently graded skin–core structure. Such a structure enables a more homogeneous stress transfer and dispersion, allowing different parts of the monofilament to deform cooperatively and share the load under tension.[26] Consequently, the PET/PBT-2% monofilament exhibited the best overall mechanical performance on the macroscale, with its structural uniformity serving as the key microstructural origin of the performance improvement.

CONCLUSIONS

This study systematically investigated the influence of PBT content on the structure and properties of PET/PBT-blended chips and monofilaments. These results indicate that PET and PBT exhibit good compatibility in the amorphous region across all compositions. At a PBT content of 2 wt%, the comprehensive mechanical properties of the PET/PBT monofilaments were significantly improved, achieving toughening of monofilaments without transesterification, along with a uniform radial orientation of molecular chains. When the PBT content reached or exceeded 5 wt%, the content of the flexible chain segments in the system increased with higher PBT loading. The crystallite sizes along the (010), (−110), and (100) planes increase from 2.4 nm, 1.7 nm, and 1.5 nm to 3.0 nm, 1.9 nm, and 1.6 nm, respectively. However, intensified transesterification leads to a decline in crystallizable and overall mechanical properties. When the PBT content exceeded 15 wt%, pronounced phase separation occurred, resulting in further degradation of the mechanical properties. The SAXS results showed no significant changes in structural parameters such as the long period, amorphous thickness, and lamellar thickness among PET/PBT monofilaments.

Conflict of Interests

The authors declare no interest conflict.

Electronic Supplementary Information

Electronic supplementary information (ESI) is available free of charge in the online version of this article at http://doi.org/10.1007/s10118-026-3673-y.

Data Availability Statement

Data will be made available on request.

ACKNOWLEDGMENTS

This work was financially supported by the National Natural Science Foundation of China (No. 52503052), Zhejiang Provincial Natural Science Foundation of China (ZJNSFC) (No. Q24E030009), General Scientific Research Project of Zhejiang Education Department (No. Y202457124), and the Science Foundation of Zhejiang Sci-Tech University (No. 25212143-Y). We are particularly grateful to beamlines BL16B1, BL14B1, and BL10U1 (Shanghai Synchrotron Radiation Facility) for providing the beam time and assistance during the experiments.

REFERENCES

1 Chen, K.; Zhang, Y.; Liu, C.; Zhang, Y.; Zhang, X. The evolution of structure and properties in high-tenacity poly(ethylene terephthalate) industrial fibers during thermal-oxidative aging process. *Polymer* **2024**, *307*, 127246.
2 Di Lorenzo, M. L. Crystallization of Poly(ethylene terephthalate): a review. *Polymers* **2024**, *16*, 1975.
3 Lei, H.; Qiu, Y.; Pan, Z.; He, B.; Yan, T. Weavable PPy/WPU/PET composite conductive fibers with high durability for multifunctional sensing applications. *Polymer* **2025**, *336*, 128886.
4 Fan, C.; Liu, Y.; Zhang, Y. A universal, highly sensitive and seamlessly integratable textile resistive strain sensor. *Adv. Fiber Mater.* **2024**, *6*, 1152–1161.
5 Su, J. juan; Peng, F.; Gao, X.; Yang, G. hui; Fu, Q.; Wang, K. Superior toughness obtained *via* tuning the compatibility of poly(ethylene terephthalate)/poly(ethylene-octene) blends. *Mater. Des.* **2014**, *53*, 673–680.
6 Song, Q. L; Wen, H. Y; de Claville Christiansen, J.; Yu, D. H; Chen, C. S; Jiang, S. C. Analysis of structure transition and compatibility of PTT/PC blend without transesterification. *Chinese J. Polym. Sci.* **2016**, *34*, 1172–1182.
7 Miao, Z.; Li, L.; Xie, Y. H; Feng, D.; Wu, F.; Xie, D.; Liu, Y.; Mei, Y. Revisiting maleic anhydride-grafted biopolymers for improved compatibility and toughening of PLA/PBAT blends: Effects of molecular weight and grafting ratio. *Polymer* **2025**, *320*, 128055.
8 Jiang, C.; Chen, P.; Mi, J.; Wang, X. PET composite foam with high stiffness and high ductility: synergistic effect of Toughener combined with simultaneous in-situ fibrillation of LCP/PTFE. *Polymer* **2025**, *333*, 128646.
9 Tan, Z.; Liu, S.; Cui, X.; Wu, G.; Sun, S.; Zhang, H. Toughening of poly(ethylene terephthalate) and optimizing of the compatibilization between PET and EPDM by functionalized EPDM. *Polym. Plast. Technol. Eng.* **2014**, *53*, 141–149.
10 Mazraeh-Shahi, Z. T.; Mojtahedi, M. R. M. Effect of blending two fiber-grade polypropylenes with different molecular weight distributions on the physical and structural properties of melt-spun filament yarns. *J. Text. Inst.* **2010**, *101*, 547–555.
11 Chen, S.; Fu, X.; Jing, Z.; Chen, H. Non-isothermal crystallization kinetics and rheological behaviors of PBT/PET blends: effects of PET property and nano-silica content. *Des. Monomers Polym.*

Graphical Abstract

Tuning the Structure and Properties of Poly(ethylene terephthalate)/Poly(butylene terephthalate) Blend Monofilaments: Mechanism of Transesterification and Gradient Structure Development

Zhong-Li Zhang, Bo-Hao Li, Jia-Ke Fan, Kang Chen, Yi-Ning Hao, Xin-Yu Liu, and Xian-Ming Zhang

Zhejiang Sci-Tech University; Zhejiang Provincial Innovation Center of Advanced Textile Technology

Poly(ethylene terephthalate)/Poly(butylene terephthalate) (PET/PBT) monofilaments were prepared by melt-blending spinning. At 2 wt% PBT, the monofilament exhibited a uniform radial-gradient structure and optimal mechanical properties. Excessive PBT induces transesterification and phase separation, thereby deteriorating performance.

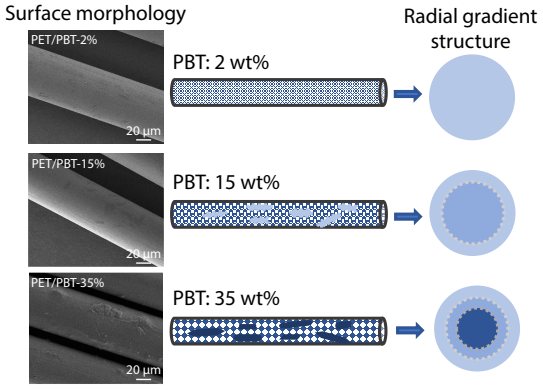

Chinese J. Polym. Sci., 2026 *https://doi.org/10.1007/s10118-026-3673-y*

2022, *25*, 32–46.

12 Mao, H. I.; Chou, J. Y.; Lin, S. Y.; Wang, C. Y.; Chen, C. H.; Chen, C. W. Enhancing poly(butylene terephthalate) (PBT) fiber orientation and tenacity *via* controlled recycling of composition-tuned vitrimers. *Polymer* **2025**, *329*, 128491.

13 Marcinčin, A. Modification of fiber-forming polymers by additives. *Prog. Polym. Sci.* **2002**, *27*, 853–913.

14 Avramova, N. Amorphous poly(ethylene terephthalate)/poly(butylene terephthalate) blends: miscibility and properties. *Polymer* **1995**, *36*, 801–808.

15 Aravinthan, G.; Kale, D. D. Blends of poly(ethylene terephthalate) and poly(butylene terephthalate). *J. Appl. Polym. Sci.* **2005**, *98*, 75–82.

16 Leung, W. H.; Leitao, E. M.; Verbeek, C. J. R. Polyester transesterification through reactive blending and its applications: a comprehensive review. *Polymer* **2025**, *329*, 128488.

17 Bi, X.; Li, J.; Guo, J.; Yu, C. A novel *in-situ* crosslinking wet spinning method for promoting the strength of CNC/alginate fiber. *Polymer* **2025**, *325*, 128313.

18 Pan, D.; He, H.; Sun, J.; Cao, M.; Qin, Z.; Chen, L. Radial crystallization difference of melt-spun polypropylene fiber along spinning line. *J. Appl. Polym. Sci.* **2019**, *136*, 47175.

19 Davies, R. J.; Burghammer, M.; Riekel, C. Probing the internal structure of high-performance fibers by on-axis scanning diffractometry. *Macromolecules* **2007**, *40*, 5038–5046.

20 Perret, E.; Chen, K.; Braun, O.; Muff, R.; Hufenus, R. Radial gradients in PET monofilaments: A Raman mapping and SAXS tomography study. *Polymer* **2022**, *238*, 124422.

21 Ren, H.; He, Z.; Xu, J.; Yan, X.; Liu, P. Evaluation of the abilities of ozone resistance for polyamide fibers: structures, properties, and aging mechanism. *Ind. Eng. Chem. Res.* **2019**, *58*, 17814–17823.

22 Hahm, W. G.; Ito, H.; Kikutani, T. Structural evolution of poly(ethylene terephthalate) fibers in high-speed in-line drawing process. *Polymer* **2025**, *319*, 128010.

23 Nowicka, W.; Rozanski, A.; Pasha, F. A.; Jasinska-Walc, L.; Duchateau, R. Polyethylene-like polyesters: strategies for tailoring mechanical properties and adhesion performance. *Macromolecules* **2025**, *58*, 9440–9449.

24 Chen, X. X.; Yu, J. C.; Chen, K.; Ji, P.; Chen, X. L.; Pan, Z. J. Facile and large-scale fabrication of biodegradable thermochromic fibers based on poly(lactic acid). *Chinese J. Polym. Sci.* **2022**, *40*, 1242–1251.

25 Ohara, A.; Kojio, K. X-ray scattering analyses on an aggregation structure of poly(ethylene terephthalate) films under bending deformation. *Macromolecules* **2024**, *57*, 3687–3695.

26 Liu, P.; Zhang, Z.; Zhu, H.; Deng, X.; Li, Z.; Li, Y.; Lv, J.; Zhang, D.; Liu, X.; Luo, L. Skin-core structural homogeneity and stress-induced ordering enable extrinsic toughening in rigid-chain heterocyclic aramid fibers. *Macromolecules* **2025**, *58*, 9358–9372.

27 Liu, C.; Zhang, Y.; Chen, K.; Li, B.; Zhang, Z.; Fan, J.; Yin, Y.; Zhang, X. Disclosing the UV aging mechanisms of polyamide 66 industrial fiber on the base of the multi-scale structural evolutions. *Polymer* **2025**, *316*, 127872.

28 Liu, S.; Li, W.; Liang, B.; Yu, Y. Chain structure and thermal behavior of reactive blends of poly(ethylene terephthalate)/poly(butylene terephthalate) by addition of 2,2′-(1,4-phenyl) bisoxazoline. *Eur. Polym. J.* **2000**, *36*, 2159–2165.

29 Newmark, R. A. Sequence distribution in polyethylene/tetramethylene terephthalate copolyesters by ^{13}C-NMR. *J. Polym. Sci. Polym. Chem. Ed.* **1980**, *18*, 559–563.

30 Wang, F.; Meng, X.; Xu, X.; Wen, B.; Qian, Z.; Gao, X.; Ding, Y.; Zhang, S.; Yang, M. Inhibited transesterification of PET/PBT blends filled with silica nanoparticles during melt processing. *Polym. Degrad. Stabil.* **2008**, *93*, 1397–1404.

31 Ucpinar Durmaz, B.; Ozturk, C.; Aytac, A. Reduced graphene oxide reinforced PET / PBT nanocomposites: compatibilization and characterization. *Polym. Eng. Sci.* **2020**, *60*, 2606–2618.

32 Yu, Y.; Choi, K. J. Crystallization in blends of poly(ethylene terephthalate) and poly(butylene terephthalate). *Polym. Eng. Sci.*

1997, *37*, 91–95.
33 Zhang, T.; Zhang, L.; Li, C. Inhibited transesterification of poly(butylene terephthalate)/poly(ethylene terephthalate)/SiO_2 nanocomposites by two processing methods. *J. Macromol. Sci. B* **2011**, *50*, 453–462.
34 Zhou, X. W.; Huang, J.; Zhang, X. H.; Li, T.; Wang, Y.; Wang, S. B.; Xia, B. H.; Dong, W. F. Design of tough, yet strong, heat-resistant PLA/PBAT blends with reconfigurable shape memory behavior by engineering exchangeable covalent crosslinks. *Chinese J. Polym. Sci.* **2023**, *41*, 1868–1878.
35 Safonov, P. E.; Levakova, N. M.; Yukhin, S. S. Evaluation of the industrial processability of high-strength and high-modulus yarns in weaving, taking into account abrasion resistance. *Fibre Chem.* **2016**, *47*, 397–402.
36 Zhang, W.; Song, H.; Liu, Y.; Chen, J.; Shi, J.; Li, L. Polyethylene-grafted poly(hexamethylene guanidine) modified ultra-high molecular weight polyethylene monofilaments and their antimicrobial properties. *R. Soc. Open Sci.* **2025**, *12*, 250340.
37 Meng, C.; Qu, J. ping. Mechanical and thermal properties of polybutylene terephthalate/ethylene-vinyl acetate blends using vane extruder. *e-Polymers* **2018**, *18*, 67–73.
38 Yamamoto, Y.; Hoshina, H.; Sato, H. Differences in intermolecular interactions and flexibility between poly(ethylene terephthalate) and poly(butylene terephthalate) studied by far-infrared/terahertz and low-frequency Raman spectroscopy. *Macromolecules* **2021**, *54*, 1052–1062.
39 Patcheak, T. D.; Jabarin, S. A. Structure and morphology of PET/PEN blends. *Polymer* **2001**, *42*, 8975–8985.
40 Heidrich, D.; Gehde, M. The 3-phase structure of polyesters (PBT, PET) after isothermal and non-isothermal crystallization. *Polymers* **2022**, *14*, 793.
41 Fan, R.; Sun, N.; Zhang, Y.; Zhang, Y. The feasibility and rationale for utilizing high molecular weight PBT in the preparation of high-strength fiber. *Polymer* **2024**, *311*, 127484.
42 Abou-Kandil, A. I.; Windle, A. H. The development of microstructure in oriented polyethylene terephthalate (PET) during annealing. *Polymer* **2007**, *48*, 5069–5079.
43 Perret, E.; Braun, O.; Sharma, K.; Tritsch, S.; Muff, R.; Hufenus, R. High-resolution 2D Raman mapping of mono- and bicomponent filament cross-sections. *Polymer* **2021**, *229*, 124011.